https://doi.org/10.5194/egusphere-2025-6490
Preprint. Discussion started: 27 February 2026
© Author(s) 2026. CC BY 4.0 License.

Optimization of snow cover fraction parameterization in the Community Land Model: implementation and preliminary validation over Tibetan Plateau

Kai Yang[1,2*], Chenghai Wang[2], Yang Cui[3*], Lingyun Ai[2], Feimin Zhang[2], Pinghan Zhaoye[2,4]

[1]Institute of Mountain Hazards and Environment, Chinese Academy of Sciences, Chengdu, 610299, China
[2]Key Laboratory of Climate Resource Development and Disaster Prevention of Gansu Province, Research and Development Center of Earth System Model, College of Atmospheric Sciences, Lanzhou University, Lanzhou 730000, China
[3]Ningxia Meteorological Bureau, Yinchuan 750002, China
[4]Changzhou Environmental Monitoring Center of Jiangsu Province, Changzhou, 213004, China

Correspondence to: Kai Yang (kaiyang@imde.ac.cn), Yang Cui(cuiyang@cma.gov.cn)

Abstract. Snow cover over Tibetan Plateau (TP) is not only a key land forcing for the regional and global climate but also an important water resource for surround regions. However, state-of-the-art climate models still exhibit substantial biases in simulating winter snow cover over the TP, which constitutes one of the major sources of uncertainty in climate prediction. Using satellite-based snow cover datasets, this study reveals that the Community Land Model version 5 (CLM5) systematically overestimates the winter snow cover fraction (SCF) over the TP. This bias mainly arises because the original SCF parameterization scheme neglects the spatially varying probability distribution of snowfall accumulation and underestimates snow depletion over barren land during the melting period. By accounting for the effects of non-growing-season low vegetation (i.e., withered grass stems) and topographic relief, we parameterize the snow accumulation probability factor (k_{accum}) instead of prescribing it as a constant. In addition, a revised factor is introduced to modify the snow depletion curve shape parameter (N_{melt}), thereby optimizing the SCF parameterization scheme. Preliminary validation indicates that the optimized scheme substantially reduces positive winter SCF biases over barren land and grassland by 34%~88%, and improves surface albedo simulations, thereby alleviating cold surface temperature biases by approximately 1~2 °C in snow-affected regions.

1 Introduction

Snow cover is a key parameter on the land surface due to its high albedo and hydrological effects of snowmelt, greatly affecting the surface energy balance and water cycle, plays an important role in climate system (e.g., Wang et al., 2017; Henderson et al., 2018; Yang et al., 2023). Accurate parameterization of snow cover is critical for the performance of numerical models in weather and climate simulations and predictions, particularly in high-latitude and high-altitude regions (Toure et al., 2016). Previous studies have indicated that biases in simulated snow cover over the Tibetan Plateau (TP) are among the primary

https://doi.org/10.5194/egusphere-2025-6490
Preprint. Discussion started: 27 February 2026
© Author(s) 2026. CC BY 4.0 License.

causes of errors in local near-surface air temperature simulations and contribute substantially to uncertainties in climate simulations over East Asia (Orsolini et al., 2019; Zhou et al., 2023). Therefore, optimizing snow cover parameterizations in land surface models (LSMs) remains essential for improving the capability of numerical models to simulate and predict weather and climate.

Over the past decades, snow cover parameterizations have been substantially developed (e.g., Niu and Yang, 2007; Swenson and Lawrence, 2012; Vionnet et al., 2012; van Kampenhout et al., 2017; Lawrence et al., 2019). In addition, considerable efforts have been made to improve simulations of snow cover and associated surface energy processes over the TP by accounting for blowing snow, complex topography, and snow albedo variations. For example, Xie et al. (2019) coupled a blowing snow model (PIEKTUK) with the Community Land Model version 4.5 (CLM4.5) and improved simulations of snow dynamics over most regions of the TP. Based on station observations and simulations with the SNICAR radiative transfer model, Wang et al. (2020) developed a fresh snow albedo scheme in the Noah-MP land surface model, which effectively reduced excessive snow depth biases over the TP. Liu and Ma (2024) further showed that an improved albedo scheme—by optimizing snow age parameters and explicitly accounting for snow depth in the Noah land surface model—enhanced snow cover simulations in the Weather Research and Forecasting (WRF) model during snow events over the TP. The Community Land Model version 5 (CLM5), the latest LSM developed by the U.S. National Center for Atmospheric Research (NCAR), incorporates substantial improvements in snow cover parameterization compared with its predecessor, CLM4 (Lawrence et al., 2019). These developments include separate calculations of snow cover fraction (SCF) for accumulation and depletion stages, representations of topographic effects on snowmelt, and the influence of wind and air temperature on fresh snow density (van Kampenhout et al., 2017). Nevertheless, pronounced biases in snow cover simulations persist over high-latitude regions and the TP in both CLM4 (Toure et al., 2016) and CLM5 (Ma and Wang, 2022). Moreover, cold surface temperature biases over the TP remain evident in most CMIP6 models (Cui et al., 2021). Thus, further comprehensive improvements to snow cover parameterizations are still required, even in the latest and relatively well-developed LSMs.

In LSMs, one of the largest sources of uncertainty in simulating snow cover and the surface energy budget arises from snow cover fraction (SCF) parameterizations (Niu and Yang, 2007; Swenson and Lawrence, 2012). Traditionally, SCF parameterizations are formulated based on the relationship between SCF and snow depth, with empirical parameters introduced to represent subgrid-scale variability and surface heterogeneity (Liston, 2004). Over the TP, the land surface exhibits pronounced spatial heterogeneity, characterized by large topographic relief and diverse low-stature vegetation. Previous studies have investigated the influence of topography on SCF (e.g., Douville et al., 1995; Lopez-Moreno and Stähli, 2008). Recently, Miao et al. (2022) demonstrated that SCF simulation biases in the Simplified Simple Biosphere Model version 3 (SSiB3) can be reduced by accounting for topographic effects, suggesting that more complex terrain tends to produce a smaller snow-covered extent for a given amount of snow. In contrast, Zhang et al. (2022) showed that incorporating a three-dimensional subgrid terrain radiative effect scheme effectively diminishes the overestimation of surface solar radiation and alleviates warm land surface temperature biases, highlighting the shading and cooling effects of complex terrain. This implies that increased topographic complexity may also retard snowmelt. Therefore, the effects of topography on snow cover appear

https://doi.org/10.5194/egusphere-2025-6490
Preprint. Discussion started: 27 February 2026
© Author(s) 2026. CC BY 4.0 License.

to be twofold, yet this dual role is not fully represented in current LSMs. In addition, snow cover over most regions of the TP is generally shallow, such that low vegetation—particularly withered grass stems (WGS) and branches over the southern and eastern TP—is not completely buried by snow. Recent studies have suggested that WGS can enhance snowmelt over the TP by altering surface energy exchange processes (Yang et al., 2023; Qi et al., 2024), an effect that is largely neglected in existing LSMs. Consequently, how to explicitly incorporate the influences of pronounced topographic relief and WGS into SCF parameterizations remains a challenging but critical issue.

This study addresses two main objectives. First, it investigates the characteristics of winter snow cover simulation biases over the TP in CLM5 and explores their potential causes from the perspective of deficiencies in the SCF parameterization. Second, it seeks to optimize the SCF parameterization by comprehensively accounting for the effects of topography and WGS. The remainder of this paper is organized as follows. Section 2 describes the data and methodology. Section 3 presents the optimization of the SCF parameterization and the experimental design used to evaluate both the original and optimized schemes. Section 4 reports the model results, including an analysis of winter snow cover biases simulated by CLM5, validation of the optimized scheme, and its impacts on the surface energy budget. Section 5 discusses uncertainties related to snowfall in LSMs and remaining challenges. Finally, conclusions are presented in Section 6.

2 Data and Methods

2.1 Meteorological forcing and validation dataset

To conduct the offline simulation of CLM5 over TP, the 3-hourly China meteorological forcing dataset v1.6 (CMFD 1.6; https://data.tpdc.ac.cn/zh-hans/data/8028b944-daaa-4511-8769-965612652c49/) (Yang et al., 2010; He et al., 2020) with a horizontal resolution of 0.1° × 0.1° for the period 1979–2018 was obtained, CMFD 1.6 includes the surface air temperature, surface pressure, specific humidity, wind speed, precipitation, downward shortwave and longwave radiation.

To validate the CLM5 simulations of snow cover over TP, a daily cloudless Moderate Resolution Imaging Spectroradiometer (MODIS) snow area ratio dataset (2000-2015) with the 500 m spatial resolution (https://data.tpdc.ac.cn/en/data/94a8858b-3ace-488d-9233-75c021a964f0/) was obtained, this dataset is obtained by using a cloud removal algorithm based on cubic spline interpolation (Tang et al., 2013). A daily, 0.05° snow depth dataset for TP (2000-2021) (https://data.tpdc.ac.cn/en/data/0515ce19-5a69-4f86-822b-330aa11e2a28/) was also used, which is obtained based on the sub-pixel spatio-temporal downscaling algorithm and the fusion of snow cover probability dataset and Long-term snow depth dataset in China (Yan et al., 2022).

To analyze the effects of the optimized SCF parameterization scheme on surface energy budget, the Global Land Surface Satellites (GLASS) albedo products (Liang et al., 2021; https://glass.hku.hk/archive/Albedo/MIX/0.05D/) with a 0.05° × 0.05° spatial resolution and 8-day temporal resolution from 2002 to 2011 was used, and the monthly data was

https://doi.org/10.5194/egusphere-2025-6490
Preprint. Discussion started: 27 February 2026
© Author(s) 2026. CC BY 4.0 License.

averaged from it. The MODIS monthly land surface temperature product with a 0.05° × 0.05° spatial resolution from 2002 to 2011 was also used (https://ladsweb.modaps.eosdis.nasa.gov/missions-and-measurements/products/MOD11C3).

The 0.05° × 0.05° dataset was averaged to the 0.1° × 0.1° for the convenient comparison with CLM5 simulations.

2.2 Standard deviation of topography and stem area index (SAI) dataset

In this study, the grid cell standard deviation of topography for the SCF parameterization was calculated based on the elevation data obtained from the USGS HYDRO1K 1-km dataset (Verdin and Greenlee, 1996; https://doi.org/10.5066/F77P8WN0). The SAI data which is used as the proxy of WGS area or coverage is derived from a MODIS consistent land surface parameters dataset (Lawrence and Chase, 2007; https://svn-ccsm-inputdata.cgd.ucar.edu/trunk/inputdata/lnd/clm2/mappingdata/grids/).

2.3 Validation metrics

The mean bias error (MBE) was used to quantify the errors of model simulations, which is calculated as follows:

$$MBE = \frac{1}{n}\sum_{i=1}^{n}\left(x_{s,i} - x_{o,i}\right) \quad (1)$$

where $x_{s,i}$ and $x_{o,i}$ represent the simulated value and observed value, respectively, n represents the sequence length.

2.4 Selection of daily snowfall events and snowmelt events

In this study, the SCF parameterization is optimized separately for snowfall and snowmelt processes at a daily timescale. Accordingly, daily snowfall and snowmelt events need be identified.

Because direct observations of snowfall are unavailable, daily positive changes in snow depth are used as a proxy to identify the occurrence and approximate magnitude of snowfall. For each year during the period 2003–2012 (10 years), the 10 days with the largest increases in snow depth are selected, yielding a total of 100 snowfall events. These snowfall amounts are then sorted from the smallest to the largest, and the resulting sequence is treated as a continuous snow accumulation process.

Similarly, daily negative changes in snow depth are adopted as a proxy for snowmelt. For each year from 2003–2012, the 10 days with the largest decreases in snow depth are selected, resulting in a total of 100 snowmelt events. These snowmelt amounts are subsequently sorted from the largest to the smallest, and the ordered sequence is regarded as a continuous snow depletion process.

https://doi.org/10.5194/egusphere-2025-6490
Preprint. Discussion started: 27 February 2026
© Author(s) 2026. CC BY 4.0 License.

It is acknowledged that daily changes in snow depth do not strictly represent actual snowfall and snowmelt amounts. However, the associated uncertainties are considered acceptable, as these quantities are not directly used in the SCF calculations.

3 SCF parameterization optimization and experimental design

3.1 Current SCF parameterization in CLM5

This study adopted CLM5 which was well developed in descriptions of surface energy fluxes and hydrology processes (Lawrence et al., 2019). In CLM5, the parameterization of SCF (f_{snow}) is based on the method of Swenson and Lawrence (2012). Because the processes governing snowfall and snowmelt differ, changes in f_{snow} are calculated separately for accumulation and depletion. When snowfall occurs, f_{snow} is updated as

$$f_{snow}^{n+1} = 1 - \left(\left(1 - \tanh\left(k_{accum} q_{snow} \Delta t \right) \right) \left(1 - f_{snow}^{n} \right) \right) \tag{2}$$

where $\tanh\left(k_{accum} q_{snow} \Delta t\right)$ is the probability distribution of snow cover during snowfall, k_{accum} is the probability distribution factor, whose default value is 0.1, $q_{snow}\Delta t$ is the amount of new snow. When snow melts, f_{snow} is calculated from the depletion curve:

$$f_{snow} = 1 - \left(\frac{\cos^{-1}\left(2R_{snow} - 1 \right)}{\pi} \right)^{N_{melt}} \tag{3}$$

where R_{snow} is the ratio of W_{snow} to the maximum accumulated snow W_{max}, and N_{melt} is the depletion curve shape parameter, which depends on the topographic variability within the grid cell:

$$N_{melt} = \frac{200}{\min\left(10, \sigma_{topo} \right)} \tag{4}$$

where σ_{topo} is the standard deviation of topography within a grid cell.

3.2 Optimizing SCF parameterization during snowfall by parameterizing the probability distribution coefficient (k_{accum})

According to Eq. (2), the value of k_{accum} determines the accumulation rate of the snow cover fraction (SCF): smaller k_{accum} values lead to slower accumulation rates and smaller SCF, even under the same snowfall amount (Figure 1a). However, in the current scheme, k_{accum} is treated as a constant with a default value of 0.1. In reality, different underlying surface types (e.g. barren, grass, shrub) are expected to influence the probability distribution of snow during snowfall. In

https://doi.org/10.5194/egusphere-2025-6490
Preprint. Discussion started: 27 February 2026
© Author(s) 2026. CC BY 4.0 License.

other words, k_{accum} should vary spatially rather than remain constant. Therefore, the current scheme likely fails to adequately represent the effects of underlying surface heterogeneity on snow accumulation.

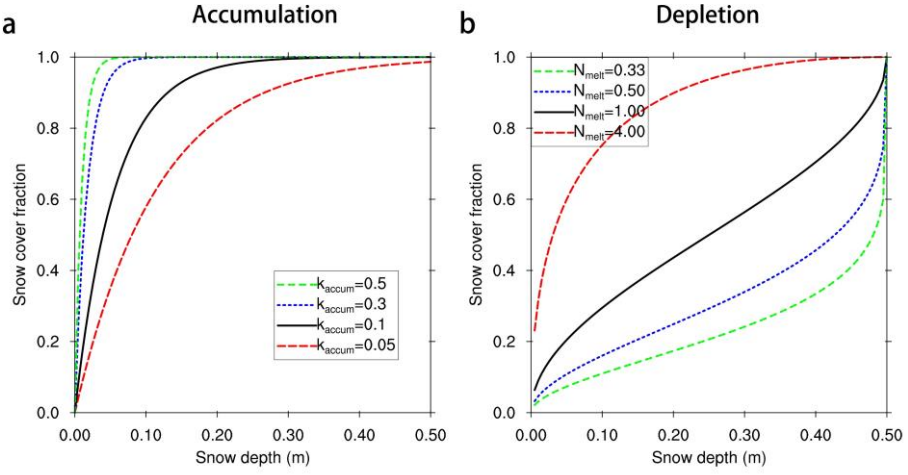

Figure 1. Relationship between snow cover fraction (SCF) and snow depth. (**a**) Accumulation curves of SCF with increase of snow depth (d_{snow}) during snowfall under different values of probability distribution factor (k_{accum}) according to equation (2), here, amount of new snow ($q_{snow}\cdot\Delta t$) is calculated by multiplying Δd_{snow} by snow density (ρ_{snow}). (**b**) Depletion curves of SCF under different values of N_{melt} according to equation (3).

To estimate optimal values of k_{accum} under different land cover types, topographic relief, and vegetation conditions (Figure 2), eight subregions were selected across the western, central, and eastern TP. As shown in Figure 2a, barren land and alpine grassland dominate most areas of the TP. Accordingly, four subregions (A–D) were selected in barren land and another four subregions (E–H) in alpine grassland. Each subregion was further divided into four panels, resulting in a total of 32 panels (Figure 2b). These panels exhibit distinct differences in topographic relief (σ_{topo}) and SAI (Figure 2c–e). Together, these variations effectively represent the heterogeneity of underlying surface conditions across the TP. It should be noted that, current SCF scheme in CLM5 mainly considered effects of large topographic relief (σ_{topo} >200m) on snowmelt (Swenson and Lawrence, 2012), while neglecting the fact that smaller topographic relief can also induce substantial SCF simulation biases (Miao et al., 2022). Therefore, σ_{topo} values in the selected panels are generally smaller than 200 m, and this study focused on effects of topography at this scale.

https://doi.org/10.5194/egusphere-2025-6490
Preprint. Discussion started: 27 February 2026
© Author(s) 2026. CC BY 4.0 License.

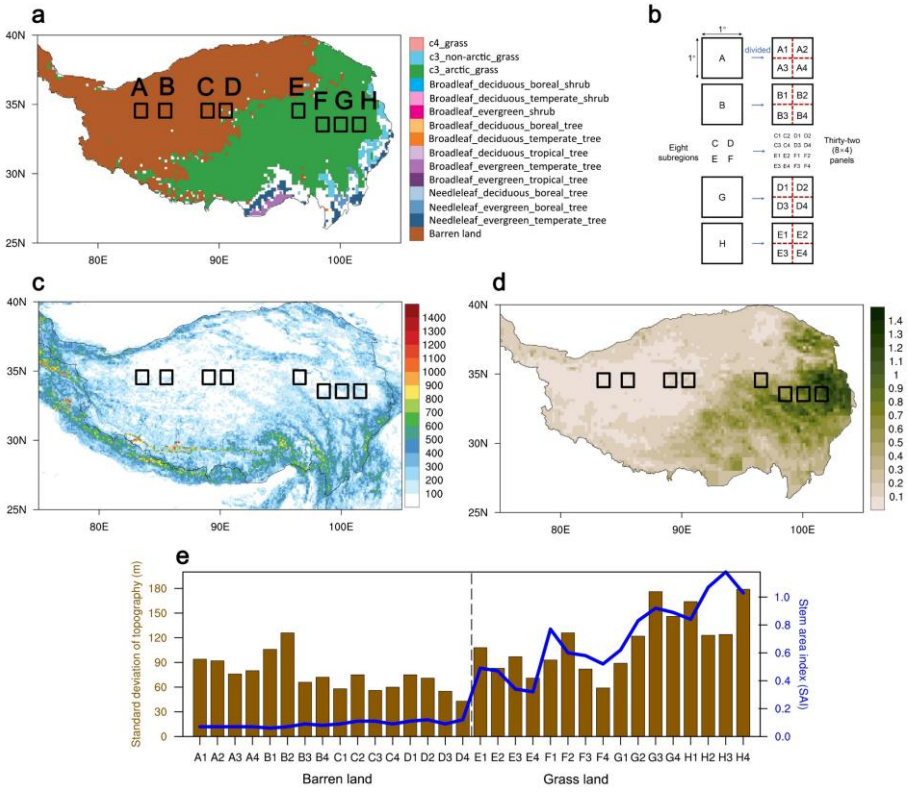

Figure 2. Subregions selected for analysis. (**a**) Underlying surface type over TP, black rectangles represent eight subregions selected for analysis. (**b**) Schematic diagram of dividing eight subregions into thirty-two panels. Spatial distribution of (**c**) standard deviation of topography (σ_{topo}; m) within a grid cell, (**d**) stem area index (SAI) in October over TP. (**e**) Evolution of σ_{topo} and SAI across thirty-two panels.

Through judging the smallest RMSE between observed SCF and the fitted value, the optimal values of k_{accum} were estimated in 32 panels during snowfall (Figure 3, Table 1). Over barren land, the optimal k_{accum} spans from 0.06 to 0.17, k_{accum} generally decreases with the larger σ_{topo}, and the averaged optimal k_{accum} is close to the default value of 0.1. Whereas, over alpine grassland, the optimal k_{accum} mostly exceeds 0.1, which varies with σ_{topo} and SAI. Comparison between the optimal k_{accum} and the default, the original scheme should overestimate the SCF over areas with small σ_{topo}, while the SCF over the alpine grassland is underestimated. Thus, above results demonstrate the values of k_{accum} should not be a constant, revealing pronounced spatial differences.

https://doi.org/10.5194/egusphere-2025-6490
Preprint. Discussion started: 27 February 2026
© Author(s) 2026. CC BY 4.0 License.

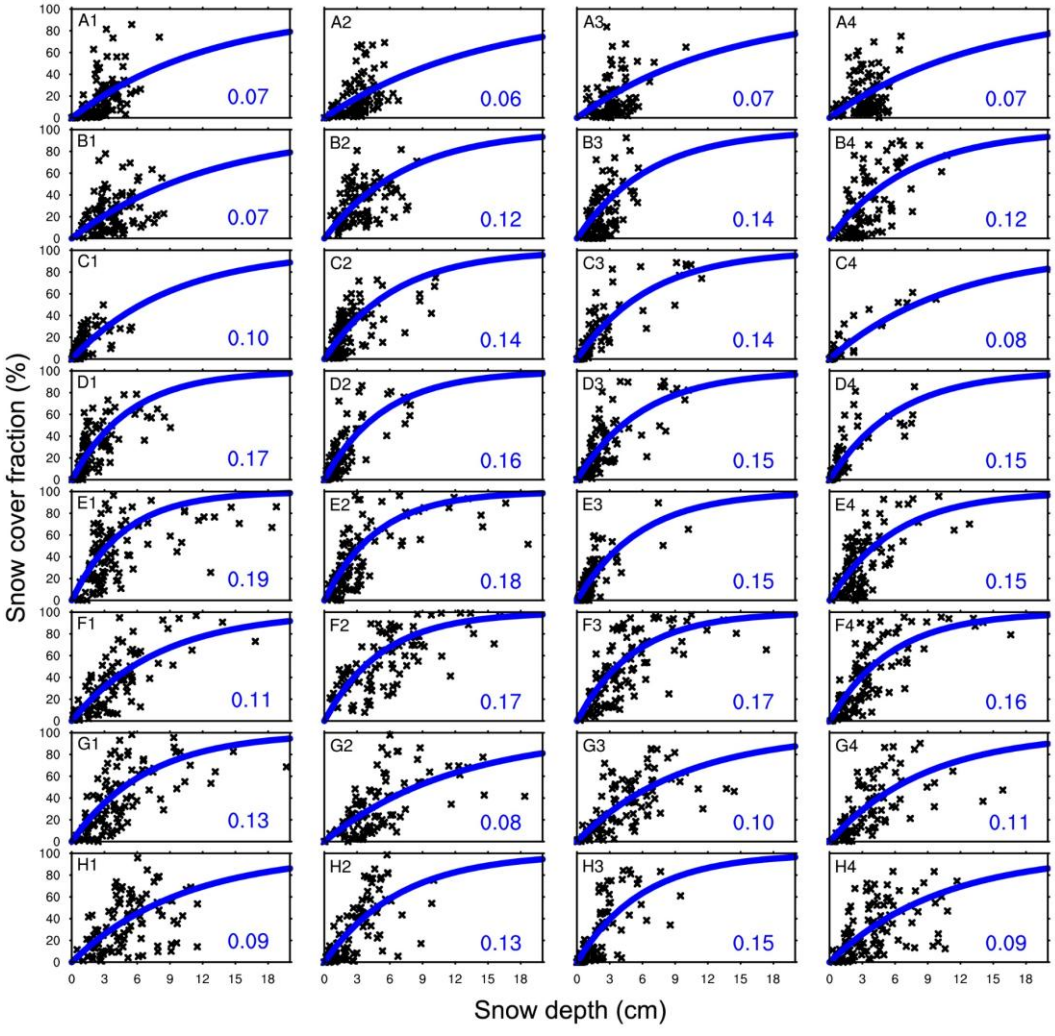

Figure 3. Relationship between snow cover fraction (SCF; %) and snow depth (cm) in 0.1×0.1 grid cells of thirty-two panels during snowfall over TP. Black circles stand for observations. The fitted lines are computed from equation (2) with the optimal values of k_{accum} (blue font numbers) which were estimated when RMSE between observed SCF and the fitted value are smallest.

Table 1. Comparison between the optimal k_{accum} ($k_{accum,optimal}$) and the default ($k_{accum,default}$) with different σ_{topo} and SAI over barren and grassland.

	Panels	σ_{topo}	SAI	$k_{accum,optimal}$	$k_{accum,default}$
Barren land	A1	94	0.07	0.07	0.1
	A2	92	0.07	0.06	
	A3	76	0.07	0.07	
	A4	80	0.07	0.07	
	B1	106	0.06	0.07	

https://doi.org/10.5194/egusphere-2025-6490
Preprint. Discussion started: 27 February 2026
© Author(s) 2026. CC BY 4.0 License.

	B2	126	0.07	0.12
	B3	66	0.09	0.14
	B4	72	0.08	0.12
	C1	58	0.09	0.10
	C2	75	0.11	0.14
	C3	56	0.11	0.14
	C4	60	0.09	0.08
	D1	75	0.11	0.17
	D2	71	0.12	0.16
	D3	55	0.09	0.15
	D4	43	0.12	0.15
Grassland	E1	108	0.49	0.19
	E2	83	0.47	0.18
	E3	97	0.34	0.15
	E4	71	0.32	0.15
	F1	93	0.77	0.11
	F2	126	0.6	0.17
	F3	82	0.58	0.17
	F4	59	0.52	0.16
	G1	89	0.62	0.13
	G2	122	0.83	0.08
	G3	176	0.92	0.10
	G4	146	0.89	0.11
	H1	164	0.84	0.09
	H2	123	1.07	0.13
	H3	124	1.18	0.15
	H4	179	1.03	0.09

To describe the spatial diversity of k_{accum}, we further parameterized k_{accum} through quantifying relationship between the optimal value of k_{accum} and σ_{topo}, SAI (Figure 4). Finally, we obtained the calculation formula of k_{accum} over the barren land and grassland as the following equation

https://doi.org/10.5194/egusphere-2025-6490
Preprint. Discussion started: 27 February 2026
© Author(s) 2026. CC BY 4.0 License.

$$k_{accum}=\begin{cases}1.15\times\sigma_{topo}^{-0.55} & \text{Barren land}\\ -5\times10^{-4}\times\left(\sigma_{topo}\times SAI\right)+0.18 & \text{Grass land}\end{cases} \quad (5)$$

Then, equation (5) was combined with equation (2) and the optimized SCF parameterization during snowfall was yielded as follows

$$f_{snow}^{n+1}=\begin{cases}1-\left(\left(1-\tanh\left[\left(1.15\times\sigma_{topo}^{-0.55}\right)\times q_{snow}\Delta t\right]\right)\left(1-f_{snow}^{n}\right)\right) & \text{Barren land}\\ 1-\left(\left(1-\tanh\left[\left(-5\times10^{-4}\times\left(\sigma_{topo}\times SAI\right)+0.18\right)\times q_{snow}\Delta t\right]\right)\left(1-f_{snow}^{n}\right)\right) & \text{Grass land}\end{cases} \quad (6)$$

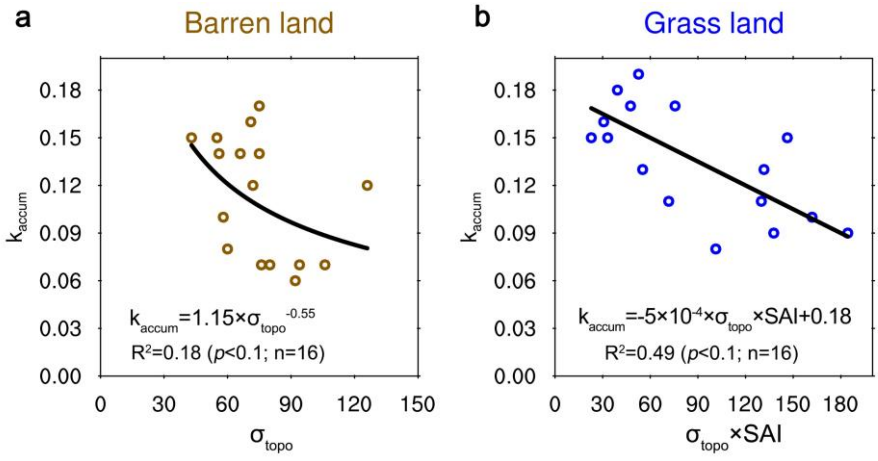

Figure 4. Relationship between the optimal value of k_{accum} and σ_{topo}, SAI over (**a**) barren land, (**b**) grassland.

3.3 Revising snow depletion curves by modifying parameterization of the shape parameter (N_{melt})

Studies suggested the WGS can warm ground (Domine et al., 2022) and benefit the melting of snow over TP (Yang et al., 2023; Qi et al., 2024). Furthermore, effect of topographic shadowing should be also considered. Therefore, it needs to estimate the optimal value of N_{melt} over the different underlying surface of TP and revise N_{melt} parametrization.

The selected eight subregions and the divided thirty-two panels were used for analysis. The optimal value of N_{melt} was estimated in snowmelt events over each panel through judging the smallest RMSE between observed SCF and fitted value (Figure 5). We can see that the optimal value of N_{melt} is obviously smaller than the original value based on the original scheme in CLM5 (Table 2), which means the current scheme should underestimate snow melting rate.

To revise parameterization of N_{melt}, here, we defined a revised factor F which is calculated as

$$F=N_{melt,optimal}/N_{melt,original} \quad (7)$$

It can be seen that, value of the revised factor F is generally less than 1 (Table 2), which implies lager melting rate over flat barren land and the positive effect of WGS on melting of snow over alpine grassland.

https://doi.org/10.5194/egusphere-2025-6490
Preprint. Discussion started: 27 February 2026
© Author(s) 2026. CC BY 4.0 License.

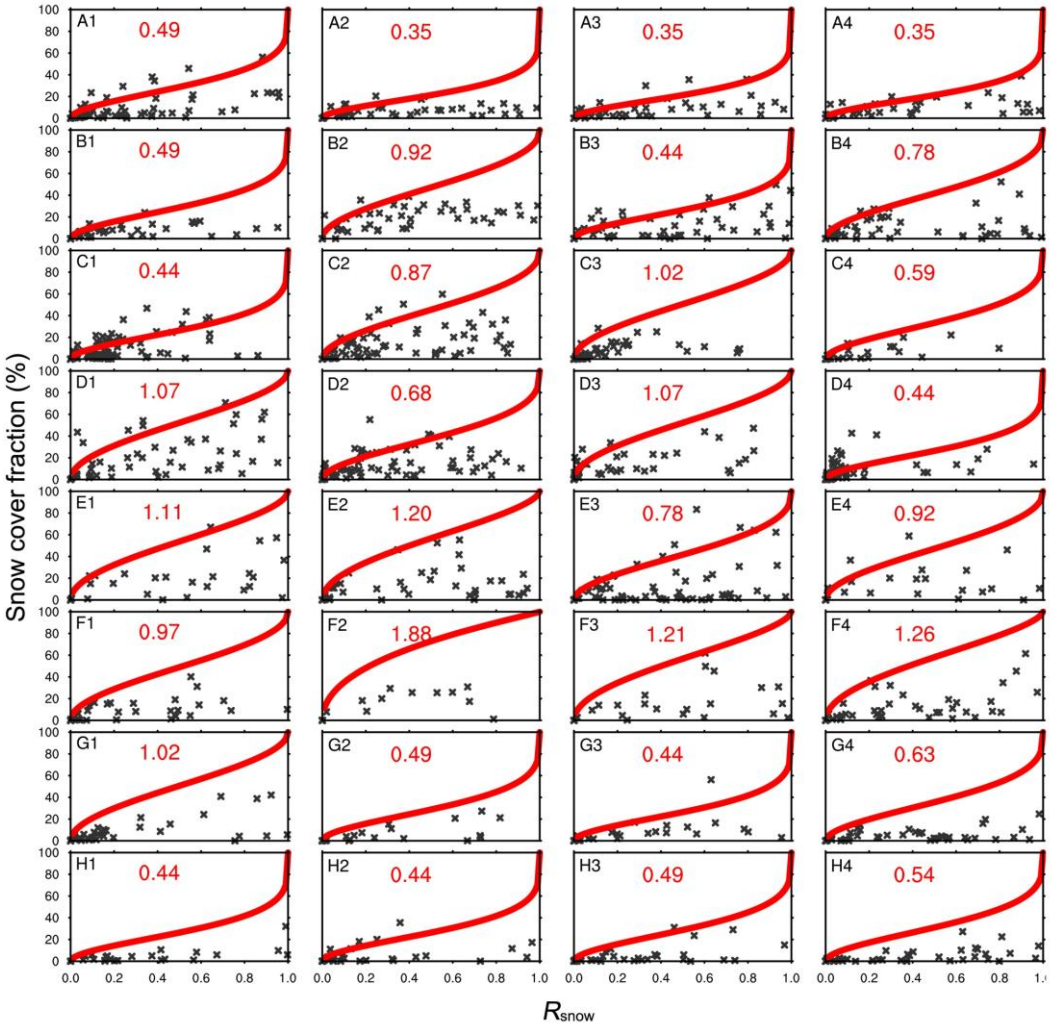

Figure 5. Relationship between snow cover fraction (SCF; %) and R_{snow} in 0.1×0.1 grid cells of thirty-two panels during snow melt over TP. Black circles stand for observations. The fitted lines are computed from equation (3) with the optimal values of N_{melt} (red font numbers) which were estimated when RMSE between observed SCF and fitted value are smallest.

Table 2. Comparison between the optimal N_{melt} ($N_{melt,optimal}$) and the original N_{melt} ($N_{melt,original}$ which was calculated from equation (4)) with different σ_{topo} and SAI over barren and grassland**.**

	Panels	σ_{topo}	SAI	$N_{melt,optimal}$	$N_{melt,original}$	Revised factor (F)
Barren land	A1	94	0.07	0.49	2.13	0.23
	A2	92	0.07	0.35	2.18	0.16
	A3	76	0.07	0.35	2.63	0.13
	A4	80	0.07	0.35	2.49	0.14
	B1	106	0.06	0.49	1.88	0.26

https://doi.org/10.5194/egusphere-2025-6490
Preprint. Discussion started: 27 February 2026
© Author(s) 2026. CC BY 4.0 License.

	B2	126	0.07	0.92	1.58	0.58
	B3	66	0.09	0.44	3.01	0.15
	B4	72	0.08	0.78	2.78	0.28
	C1	58	0.09	0.44	3.45	0.13
	C2	75	0.11	0.87	2.67	0.33
	C3	56	0.11	1.02	3.57	0.29
	C4	60	0.09	0.59	3.33	0.18
	D1	75	0.11	1.07	2.67	0.40
	D2	71	0.12	0.68	2.82	0.24
	D3	55	0.09	1.07	3.64	0.29
	D4	43	0.12	0.44	4.65	0.09
Grassland	E1	108	0.49	1.11	1.85	0.60
	E2	83	0.47	1.21	2.40	0.50
	E3	97	0.34	0.78	2.06	0.38
	E4	71	0.32	0.92	2.81	0.33
	F1	93	0.77	0.97	2.15	0.45
	F2	126	0.6	1.88	1.59	1.18
	F3	82	0.58	1.21	2.44	0.50
	F4	59	0.52	1.26	3.39	0.37
	G1	89	0.62	1.02	2.25	0.45
	G2	122	0.83	0.49	1.64	0.30
	G3	176	0.92	0.44	1.14	0.39
	G4	146	0.89	0.63	1.37	0.46
	H1	164	0.84	0.44	1.22	0.36
	H2	123	1.07	0.44	1.63	0.27
	H3	124	1.18	0.49	1.61	0.30
	H4	179	1.03	0.54	1.12	0.48

Relationship between the revised factor F and σ_{topo}, SAI was further quantified over barren and grassland (Figure 6). It can be seen that, over barren land, F increases with larger σ_{topo}, in other words, snow melt over the flat barren land should be faster than that over the complex topography, which might be due to the effect of topographic shadowing under the patched and shallow snow condition over the TP. Over alpine grassland, F decreases with larger SAI and smaller, implying

https://doi.org/10.5194/egusphere-2025-6490
Preprint. Discussion started: 27 February 2026
© Author(s) 2026. CC BY 4.0 License.

more WGS can lead to faster snow melt, which is consistent with results of previous studies (Domine et al., 2022; Yang et al., 2023; Qi et al., 2024).

To revised N_{melt} parametrization, effects of topography and WGS were combined to fit the calculation formula of F as follows

$$F = \begin{cases} 10^{-3} \times \left(3.3 \times \sigma_{topo} - 9.5\right) & \text{Barren land} \\ 0.49 \times e^{-0.004 \times \left(10^4 \times SAI^2 / \sigma_{topo}\right)} & \text{Grass land} \end{cases} \quad (8)$$

$$N_{melt,revised} = \frac{200}{\min\left(10, \sigma_{topo}\right)} \times F \quad (9)$$

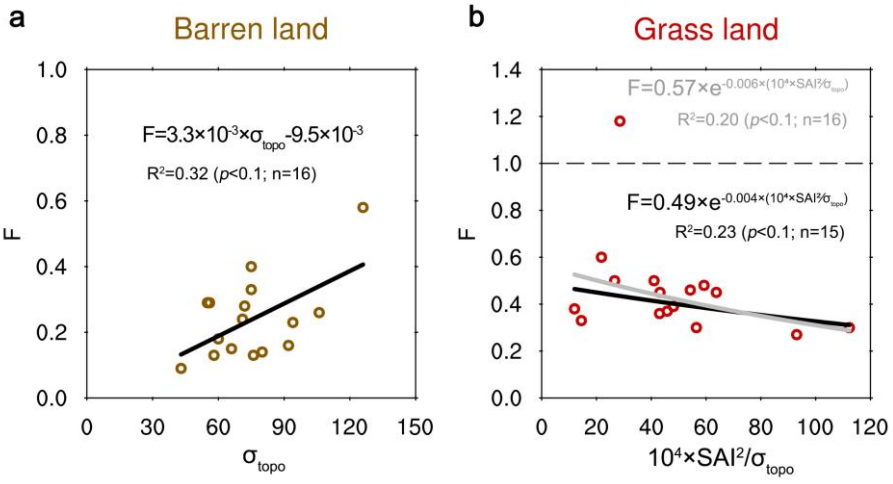

Figure 6. Relationship between the revised factor F and σ_{topo}, SAI over (**a**) barren land, (**b**) grassland. The grey and black lines in (b) represent the fitting with and without the F>1 sample.

Combining equations (8), (9) with equations (4), the optimized SCF parameterization during snowmelt was yielded as follows

$$f_{snow} = \begin{cases} 1 - \left(\dfrac{\cos^{-1}\left(2R_{snow} - 1\right)}{\pi} \right)^{\frac{200}{\min\left(10, \sigma_{topo}\right)} \times \left[10^{-3} \times \left(3.3 \times \sigma_{topo} - 9.5\right)\right]} & \text{Barren land} \\ 1 - \left(\dfrac{\cos^{-1}\left(2R_{snow} - 1\right)}{\pi} \right)^{\frac{200}{\min\left(10, \sigma_{topo}\right)} \times \left[0.49 \times e^{-0.004 \times \left(10^4 \times SAI^2 / \sigma_{topo}\right)}\right]} & \text{Grass land} \end{cases} \quad (10)$$

3.4 Experimental design

To evaluate and optimize SCF parameterization, three offline experiments were conducted using CLM5 over the TP (25°N–40°N, 75°E–105°E; Figure 2a) at a spatial resolution of 0.1° × 0.1° (Table 3). One is the control experiments (CTL),

https://doi.org/10.5194/egusphere-2025-6490
Preprint. Discussion started: 27 February 2026
© Author(s) 2026. CC BY 4.0 License.

with SCF parametrizations using the original scheme. The other two are the MOD1 and MOD2, in MOD1, SCF parametrization adopts the optimized scheme, while in MOD2, SCF parameterization only during snow melt adopts the optimized scheme. Through comparing simulations between MOD1 and MOD2, performance of the optimized scheme during snowfall and snow melt can be separately validated. The simulations cover the period from 1979 to 2018, with a model time step of 1800s and monthly output frequency. The meteorological forcing data are derived from the CMFD v1.6 (see Section 2.1 for details). The first 23 years (1979–2001) were used for a spin-up to satisfy the model equilibrium, and rest simulations during 2002–2011 used for analysis.

Table 3. Description of experimental design

	SCF parameterization scheme
CTL	SCF parameterizations during snowfall and snow melt use the original scheme (equation (2), (3))
MOD1	SCF parameterizations during snowfall and snow melt adopt the optimized scheme (equation (6), (10))
MOD2	SCF parameterization during snowfall is the original scheme, but SCF parameterization during snowmelt is the optimized scheme

4 Results

4.1 Characteristics of CLM5 simulated winter snow cover biases

In winter, most regions of the TP are snow covered, and snow is distributed in a patchy and fragmented manner, with SCF generally below 50% over most areas at the grid-cell scale (10 × 10 km) (Figure 7a). Except for the southeastern TP (e.g., the Nyenchen Tanglha Mountains), snow cover over the TP is generally shallow, with snow depth around or less than 10 cm (Figure 7b). Nevertheless, most LSMs exhibit poor performance in simulating such fragmented and shallow snow cover over the TP, typically overestimating snow extent (Toure et al., 2016; Orsolini et al., 2019). In contrast, CLM5 shows relatively small SCF biases over the eastern and southwestern TP, while pronounced biases occur over the northwestern TP. Specifically, positive SCF biases dominate the western and central TP, whereas negative biases are evident over the southeastern TP (Figure 7c). Regional average of SCF biases (MEB) over the whole TP, grassland and barren land are 9.79%, 3.37% and 13.13%, respectively.

SCF generally increases with the thicker snow depth, therefore, biases in SCF may be related to biases in snow depth. Indeed, the spatial pattern of snow depth biases (Figure 7d) is broadly consistent with that of SCF. but the northwestern TP does not exhibit correspondingly large snow depth biases, suggesting that the pronounced SCF biases in this region are

https://doi.org/10.5194/egusphere-2025-6490
Preprint. Discussion started: 27 February 2026
© Author(s) 2026. CC BY 4.0 License.

mainly attributable to deficiencies in the SCF parameterization in CLM5. Overall, CLM5 tends to overestimate winter snow cover over the TP, indicating that the SCF parameterization requires further optimization.

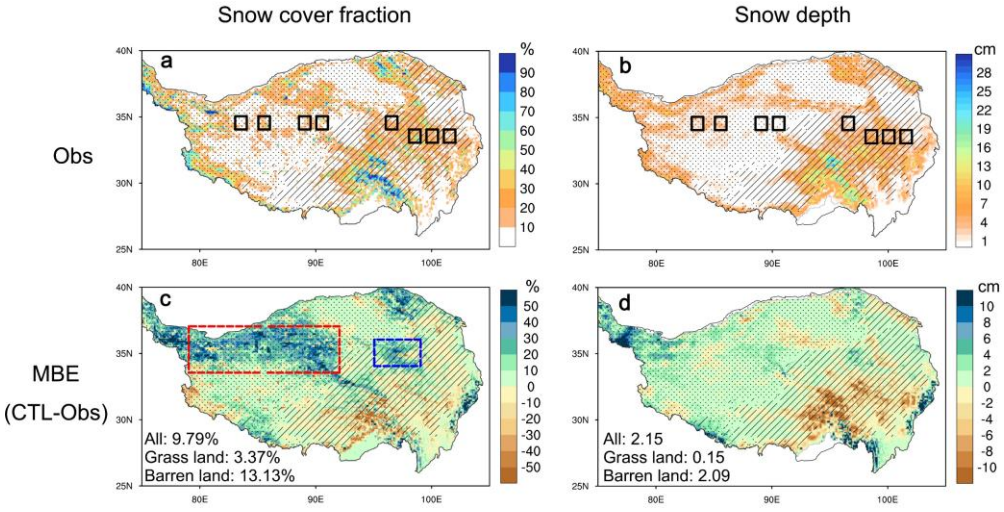

Figure 7. Distribution of winter (DJF mean) snow cover and CLM5 simulation biases. Observed (Obs) 2003-2012 averaged DJF (**a**) snow cover fraction (SCF; %), (**b**) snow depth (cm). CLM5 mean bias error (MEB; CTL-Obs) of (**c**) SCF, (**d**) snow depth during period 2003-2012. In each panel, slash shading and dot shading represent grassland and barren land, respectively. Values in (c) and (d) are MBE averaged over grid point of whole TP (All), grassland, and barren land.

4.2 Preliminary validation of the optimized SCF parameterization scheme

The details of the SCF parameterization scheme optimization by considering the impacts of WGS and topography have been detailedly introduced in section 3.2 and 3.3. Based on this framework, a preliminary validation of the optimized SCF parameterization was conducted. As shown in Figure 8a, the MEB of winter SCF simulated by the optimized scheme (MOD1) is substantially reduced, particularly over the northwestern TP, where the original scheme exhibits large biases. The regionally averaged SCF MEB over the entire TP, grassland, and barren land decreases to 5.48%, 0.40%, and 8.63%, respectively. Compared with CTL, the optimized scheme simulates less SCF over the barren and mountainous areas (Figure 8b) where the original scheme has obvious positive biases, and more SCF over the southeastern TP where the original scheme has negative biases. The relative biases of winter SCF are reduced by 34%~88%. Over the eight selected regions used for optimizing SCF parameterization, winter SCF simulation MBE from the MOD1 and MOD2 are also obviously smaller than that of the CTL (Table 4).

In CLM5, SCF during snowfall and snowmelt periods is calculated separately. Therefore, the improvements shown in the MOD1 experiment represent the combined effects of the optimized SCF scheme during both periods. To further identify which process contributes most to the improvement, simulations using the optimized SCF scheme only during the snowmelt period (i.e., the MOD2 experiment) are compared with observations CTL (Figure 8c,d). Compared with CTL, MOD2 simulates lower SCF over most regions of the TP, except for some areas with large topographic relief in the southern TP,

https://doi.org/10.5194/egusphere-2025-6490
Preprint. Discussion started: 27 February 2026
© Author(s) 2026. CC BY 4.0 License.

thereby reducing the positive SCF biases. Quantitatively, MEB of SCF averaged over the entire TP, grassland, and barren land decreases to 6.27%, 0.49%, and 8.79%, respectively. Although the reduction in SCF biases in MOD2 is slightly smaller than that in MOD1, the magnitudes of bias reduction are comparable between the two experiments. This indicates that the overall improvements achieved by the optimized SCF scheme are primarily attributable to the modifications during the snowmelt process. In the optimized SCF parameterization for the snowmelt period, the shape parameter (N_{melt}) is modified by multiplying a revised factor (F) that is less than 1. A smaller N_{melt} corresponds to a faster snow depletion rate during snowmelt (Figure 1b), which effectively reduces the positive SCF biases. In other words, the original SCF scheme underestimates the snow depletion rate, particularly over flat barren land, and the optimized scheme alleviates this deficiency to a considerable extent.

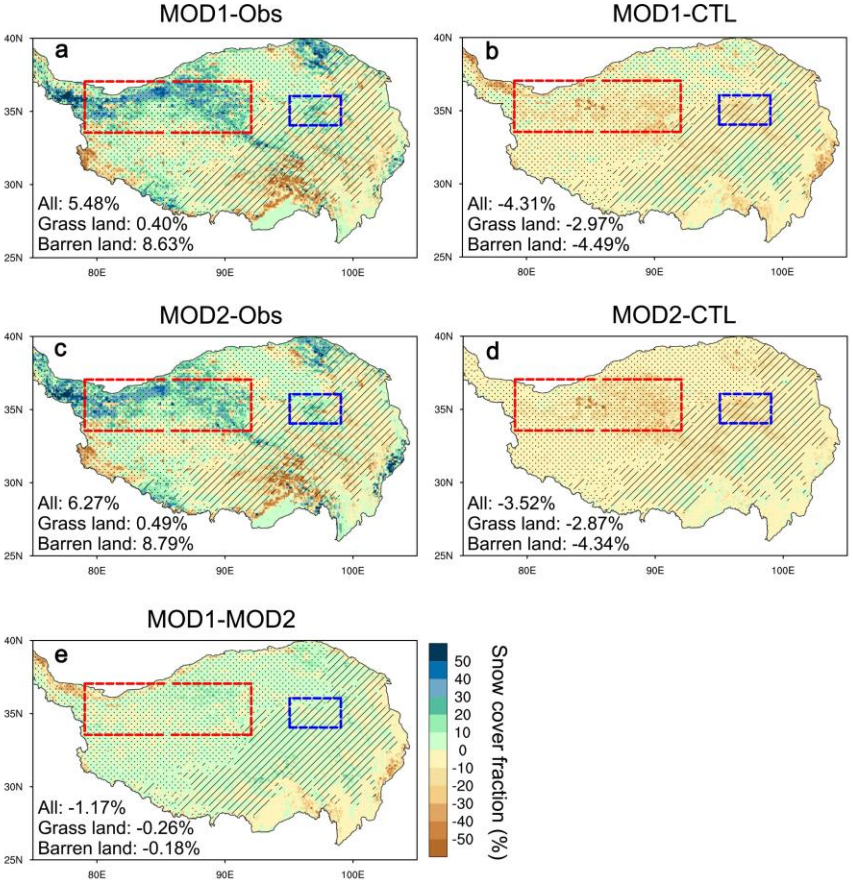

Figure 8. Comparison of simulations of SCF with modified scheme (MOD1, MOD2) with observation (Obs) and simulations with current scheme (CTL). Mean bias error (MBE) of SCF from experiments (**a**) MOD1, (**b**) differences of SCF between MOD1 and CTL. (**c**), (**d**) are same as (a), (b) but for MOD2. (**e**) Differences of SCF between MOD1 and MOD2.

For the optimized SCF parameterization scheme during snowfall, the values of the probability distribution coefficient (k_{accum}) can be greater than 1 (the default value in the original scheme) over areas with small σ_{topo} and SAI (Figure 4), which

https://doi.org/10.5194/egusphere-2025-6490
Preprint. Discussion started: 27 February 2026
© Author(s) 2026. CC BY 4.0 License.

285 means the SCF during snowfall over the flat and sparse vegetation areas calculated by the optimized scheme is larger than that of the original scheme, but smaller over the large topographic relief area. This is verified by the positive difference of SCF between the MOD1 and MOD2 (Figure 8e).

Table 4. Comparison of winter SCF simulation MBE (%) between the CTL and MOD1, MOD2.

Subregion	CTL	MOD1	MOD2
A	13.04	**0.99**	2.07
B	23.71	**9.21**	9.80
C	28.55	**18.31**	13.80
D	36.55	19.02	**17.53**
E	30.78	18.20	**15.47**
F	24.97	13.86	**12.73**
G	7.53	2.04	**1.31**
H	2.16	0.92	**0.16**

Note. The bold black values are the lowest MBE among the CTL, MOD1 and MOD2.

290 We further validated simulations in SCF evolution from winter to summer and explored the impacts of winter SCF simulation improvements on the subsequent SCF (Figure 9). Over barren land, the observed SCF reaches a maximum in February, decreases in March, and then increases again in April and May, indicating that snow accumulation over barren land in the northwestern TP occurs during both winter and spring, followed by snowmelt in summer (Figure 9a). CLM5 generally captures the monthly evolution of SCF; however, the original scheme (i.e., CTL experiment) substantially
295 overestimates winter SCF, with values more than twice those observed. In contrast, SCF simulated with the optimized scheme (MOD2) agrees much better with observations from December to March, despite a slight underestimation from April to June. Over grassland, the observed SCF accumulates in winter and reaches the maximum in February, then decreases due to the snowmelt (Figure 9b). And, the optimized scheme also shows distinct improvements in SCF simulations over grassland in the eastern TP, particularly from December to February.

https://doi.org/10.5194/egusphere-2025-6490
Preprint. Discussion started: 27 February 2026
© Author(s) 2026. CC BY 4.0 License.

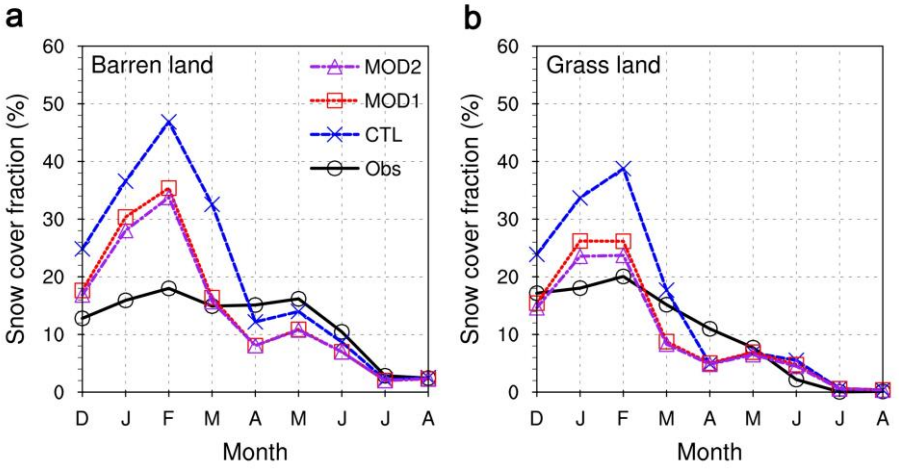

Figure 9. Comparison of simulated snow cover fraction (SCF) with observation. Evolution of SCF averaged (**a**) barren land (red rectangular box in Fig. 8), (**b**) grassland (blue rectangular box in Fig. 8).

4.3 Effects of the optimized scheme on the surface energy budget

SCF is an important factor influencing the surface albedo, which further impacts the surface energy budget. Due to the overestimation of SCF, CLM5 has obvious positive biases of surface albedo by up to 0.3 (Figure 10a), especially over the northwestern TP. And the spatial pattern of surface albedo bias is similar to that of SCF, which further confirm that winter SCF bias should be the main cause of the surface energy budget bias. While the optimized SCF scheme simulated lower surface albedo than that of the original scheme (Figure 10c), especially over the northern TP where SCF simulation is obviously improved, difference of surface albedo between MOD1 and CTL can be about -0.1, the positive biases in surface albedo are obviously reduced (Figure 10b), despite the remaining positive surface albedo bias in MOD1, which may be attributed to unresolved SCF biases and other process imperfections (such as snow albedo estimation).

https://doi.org/10.5194/egusphere-2025-6490
Preprint. Discussion started: 27 February 2026
© Author(s) 2026. CC BY 4.0 License.

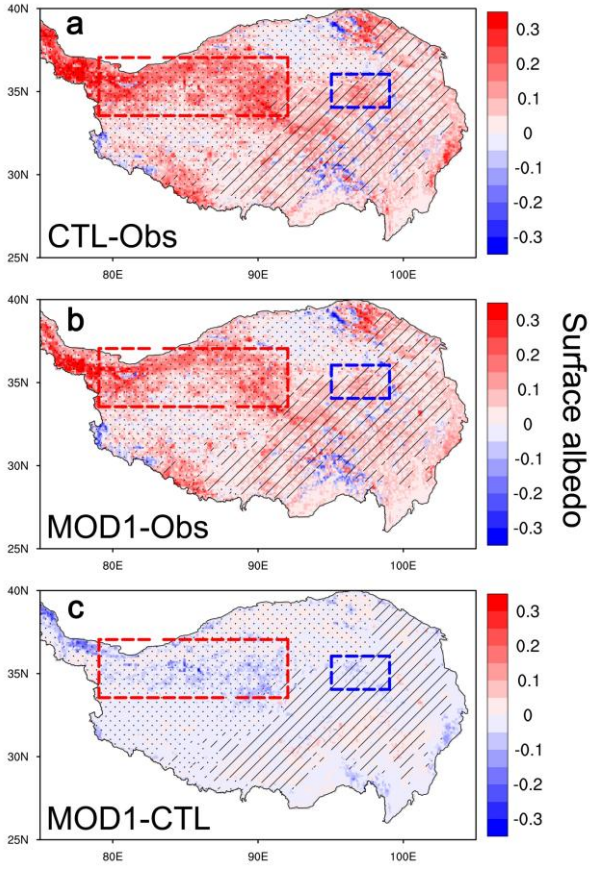

Figure 10. Differences of winter surface albedo between (**a**) CTL and observation (Obs), (**b**) MOD1 and Obs, (**c**) MOD1 and CTL.

Surface energy budget further influences the land surface temperature (LST). It has been reported that, current climate models have obviously cold biases over TP (Orsolini et al., 2019; Zhou et al., 2023), which is one of the main causes of uncertainties in simulations and projection of permafrost degeneration, surface hydrology and ecology, as well as understanding the TP thermal forcing (Xue et al., 2018; Yang et al., 2019; Ehlers et al., 2022). As excepted, CLM5 still shows cold biases (Figure 11a, b), especially over northwestern TP where snow cover fraction is overestimated, but it well reproduces spatial pattern of winter LST over TP. Compared to the original scheme, the optimized SCF scheme simulated the warmer LST (Figure 11c), in other words, the optimized SCF scheme reduces the cold bias.

Overall, the optimized SCF scheme not only improves the winter SCF simulation over TP, but also optimizes simulations of the surface energy budget to some extent.

https://doi.org/10.5194/egusphere-2025-6490
Preprint. Discussion started: 27 February 2026
© Author(s) 2026. CC BY 4.0 License.

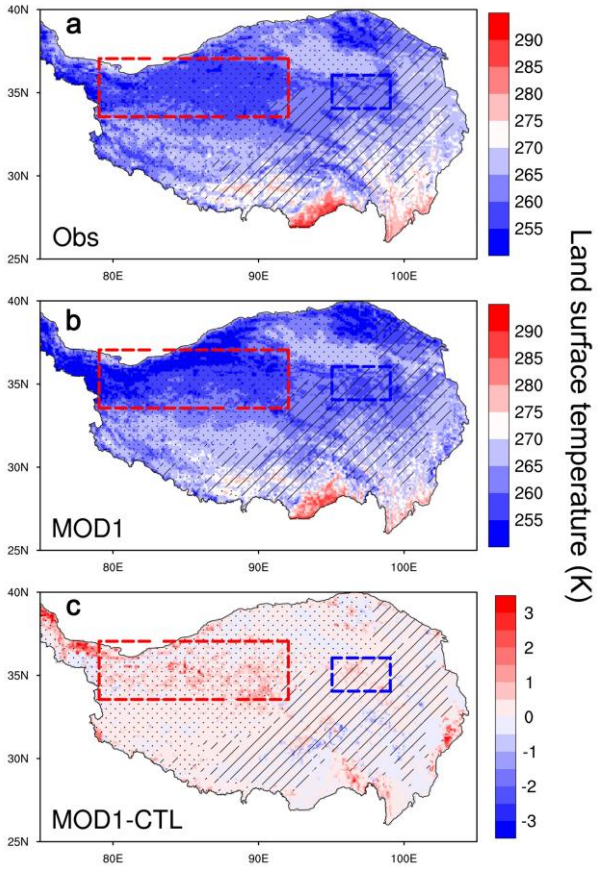

Figure 11. Evaluation of land surface temperature (LST) simulations by the modified SCF scheme. Multiyear average of LST from (**a**) observation (Obs) and (**b**)MOD1 experiment. (**c**) Difference of LST between MOD1 and CTL experiments.

5 Discussions

5.1 Uncertainty of snowfall from the meteorological forcing dataset and the parameterization scheme of total precipitation partitioning into snowfall

It has been widely recognized that biases in meteorological forcing datasets represent an important source of uncertainty in land surface process simulations (e.g., Wang et al., 2016; Zeng et al., 2021; Zhang et al., 2025), including snow cover simulations (Xie et al., 2017; Jiang et al., 2021). The formation and evolution of snow mass on the land surface involve a series of complex processes, including snowfall, accumulation, compaction, aging, and melting. In this study, we primarily focus on improving the parameterization of SCF during snowfall and snowmelt processes. Snow compaction and aging mainly affect snow albedo, which in CLM5 is simulated using the Snow, Ice, and Aerosol Radiative (SNICAR) model. At present, snowfall input to LSMs is diagnosed through parameterization schemes that partition total precipitation into rainfall and snowfall. On the one hand, due to the sparse observational network and uncertainties in reanalysis datasets over the TP,

https://doi.org/10.5194/egusphere-2025-6490
Preprint. Discussion started: 27 February 2026
© Author(s) 2026. CC BY 4.0 License.

total precipitation in meteorological forcing datasets inevitably contains biases (Liu et al., 2025). These uncertainties may contribute to the remaining snow cover biases, even after optimizing the SCF parameterization. In this study, we adopt the CMFD v1.6. Although a newer version, CMFD v2.0, has recently been released with substantial improvements—including precipitation directly derived from the TPHiPr dataset (Jiang et al., 2023)—previous evaluations indicate that CMFD v1.6 exhibits relatively lower biases compared to other forcing datasets (Liu et al., 2025). Nevertheless, a systematic assessment of the impacts of different meteorological forcing datasets on snow cover simulations over the TP remains necessary and should be addressed in future studies.

On the other hand, the parameterization scheme used to partition total precipitation into snowfall also exerts a strong influence on snow cover simulations. At present, most LSMs estimate the fraction of snowfall in total precipitation using empirical functions that rely primarily on near-surface air temperature as the independent variable. Previous studies (e.g., Leroux et al., 2023; Jennings et al., 2025) have demonstrated that the choice of precipitation phase partitioning scheme constitutes a major source of model sensitivity in simulating changes in snow mass. In CLM5, the partitioning of total precipitation into snowfall and rainfall is diagnosed using a linear ramp function. For most land units, this scheme produces all snowfall at temperatures below 0 °C, all rainfall above 2 °C, and a mixture of snowfall and rainfall at intermediate temperatures. Consequently, improving snowfall estimation in LSMs from alternative perspectives—such as incorporating crowdsourced observations of precipitation phase through data assimilation—may provide a promising pathway for further reducing uncertainties in snow cover simulations (Jennings et al., 2025).

5.2 Remaining challenge for describing the complexity of topographic relief and vegetation diversity

Due to the complexity of the underlying surface, characterized by large topographic relief and diverse vegetation, land surface modeling over the TP remains a challenging task, particularly for snow cover simulations. Over past decades, the development of LSMs has increasingly aimed to represent multiscale land surface processes in a more comprehensive manner (Prentice et al., 2015; Lu et al., 2020). In this study, the impacts of short vegetation (i.e., withered grass stems, WGS) and topography on snow cover are considered only at the grid-cell mean scale. In reality, the influence of topographic relief on snow cover is highly complex, involving both mechanical and radiative processes. Mechanical processes are manifested through snow redistribution and drifting, whereby snow tends to accumulate in gullies and depressions during snowfall. Radiative processes arise from terrain-induced three-dimensional radiation transfer, which generally leads to faster snowmelt on sun-facing slopes, while snow on shaded slopes persists for longer periods. At present, CLM5 accounts for wind effects on fresh snow density at the grid-cell scale but does not explicitly represent three-dimensional terrain radiative effects. Recent studies have demonstrated that incorporating three-dimensional terrain effects is crucial for accurately simulating land surface processes over the TP (e.g., Wang et al., 2020; Miao et al., 2022). Similarly, the influences of short vegetation on snow cover, through mechanical blocking, canopy radiative transfer, and heat conduction between vegetation stems or withered components and the snowpack, primarily operate at subgrid scales. However, the lack of high-resolution

https://doi.org/10.5194/egusphere-2025-6490
Preprint. Discussion started: 27 February 2026
© Author(s) 2026. CC BY 4.0 License.

datasets describing non-growing-season vegetation poses a major limitation for explicitly representing these processes in current LSMs. Consequently, how to more realistically describe the combined complexity of topographic relief and vegetation diversity remains an open challenge and warrants further investigation in future studies.

6 Conclusions

In this study, we evaluated the performance of CLM5 in simulating winter snow cover over TP, the original SCF parameterization scheme in CLM5 overestimates winter snow cover fraction over TP, especially over the western TP. One of the main causes is the overlooking the varied probability distribution of snow over different land surface types and underestimating the snow depletion over barren land in the original SCF parameterization scheme. Then, we optimized the SCF parameterization scheme through considering impacts of the WGS and topography to parameterize the probability distribution factor (k_{accum}) instead of the constant value, revise the depletion curve shape parameter (N_{melt}). The optimized SCF scheme obviously reduces the winter SCF simulation positive biases by 34%~88% over TP. Correspondingly, simulations in surface albedo and surface radiation budget are also improved. Results in this study provide a reference way for LSMs development over TP, which also has potential for improving local and East Asian weather and climate simulations and predictions.

https://doi.org/10.5194/egusphere-2025-6490
Preprint. Discussion started: 27 February 2026
© Author(s) 2026. CC BY 4.0 License.

Code and data availability

Code required to conduct the analyses herein is available at https://doi.org/10.5281/zenodo.18133296 (Yang, 2026).

The 3-hourly China Meteorological Forcing Dataset (CMFD) is available at https://data.tpdc.ac.cn/zh-hans/data/8028b944-daaa-4511-8769-965612652c49/ (He et al., 2020).

A daily cloudless MODIS snow area ratio dataset (2000-2015) can be obtained from https://data.tpdc.ac.cn/en/data/94a8858b-3ace-488d-9233-75c021a964f0/ (Tang et al., 2013).

A daily, 0.05° snow depth dataset for Tibetan Plateau (2000-2021) is available at https://data.tpdc.ac.cn/en/data/0515ce19-5a69-4f86-822b-330aa11e2a28/ (Yan et al., 2022).

The GLASS albedo products can be downloaded at https://glass.hku.hk/archive/Albedo/MIX/0.05D/ (Liang et al., 2021).

The MODIS monthly land surface temperature product can be obtained from https://ladsweb.modaps.eosdis.nasa.gov/missions-and-measurements/products/MOD11C3 (last access: 3 January 2026).

The USGS HYDRO1K 1-km dataset is available at https://doi.org/10.5066/F77P8WN0 (last access: 3 January 2026).

The MODIS consistent land surface parameters dataset for CLM can be download from https://svn-ccsm-inputdata.cgd.ucar.edu/trunk/inputdata/lnd/clm2/mappingdata/grids/ (last access: 3 January 2026).

CLM5 was run under the framework of Community Earth System Model version 2.2.0, which can be freely downloaded from https://github.com/ESCOMP (last access: 3 January 2026).

Author contributions

KY, CW, and YC conceived and designed the study. LA, FZ, and PZ contributed to the discussion and refinement of the research framework. KY and YC conducted the data processing and analysis and performed the sensitivity experiments with assistance from CW. KY drafted the manuscript and supervised the study, and revised the manuscript. All authors contributed to the discussion and approved the final version of the manuscript.

Competing interests

The contact author has declared that none of the authors has any competing interests.

Acknowledgements

We acknowledge the National Tibetan Plateau Data Center (TPDC) for providing the China Meteorological Forcing Dataset (CMFD), the cloudless MODIS snow cover dataset, and the Tibetan Plateau snow depth dataset used in this study. We also acknowledge NASA for providing the MODIS land surface temperature products through the LAADS DAAC, and the Global Land Surface Satellite (GLASS) project for the surface albedo products. The HYDRO1K global elevation dataset was obtained

https://doi.org/10.5194/egusphere-2025-6490
Preprint. Discussion started: 27 February 2026
© Author(s) 2026. CC BY 4.0 License.

from the U.S. Geological Survey (USGS). In addition, we acknowledge NCAR for providing the MODIS-consistent land surface parameter datasets for CLM. We appreciate the helpful discussions and assistance from colleagues that contributed to this work.

Financial support

This work was supported by National Key Research & Development Program of China (2023YFC3206300), National Natural Science Foundation of China (42305017), Key Research and Development Program Project of Ningxia Hui Autonomous Region (2024BEG03003).

References

Cui, T., Li, C., and Tian, F.: Evaluation of temperature and precipitation simulations in CMIP6 models over the Tibetan Plateau. *Earth and Space Science*, 8, e2020EA001620. https://doi.org/10.1029/2020EA001620, 2021.

Domine, F., Fourteau, K., Picard, G. et al.: Permafrost cooled in winter by thermal bridging through snow-covered shrub branches. *Nature Geoscience*, 15, 554–560. https://doi.org/10.1038/s41561-022-00979-2, 2022.

Ehlers, T. A., Chen, D., Appel, E., Bolch, T., Chen, F., Diekmann, B., et al.: Past, present, and future geo-biosphere interactions on the Tibetan Plateau and implications for permafrost. *Earth-Science Reviews*, 234, 104197. https://doi.org/10.1016/j.earscirev.2022.104197, 2022.

He, J., Yang, K., Tang, W., Lu, H., Qin, J., Chen, Y. Y., and Li, X.: The first high-resolution meteorological forcing dataset for land process studies over China. *Scientific Data*, 7(1), 25. https://doi.org/10.1038/s41597-020-0369-y, 2020.

Henderson, G.R., Peings, Y., Furtado, J.C. et al.: Snow–atmosphere coupling in the Northern Hemisphere. *Nature Climate Change*, 8, 954–963. https://doi.org/10.1038/s41558-018-0295-6, 2018.

Jennings, K. S., Collins, M., Hatchett, B. J., et al.: Machine learning shows a limit to rain-snow partitioning accuracy when using near-surface meteorology. *Nature Communications*, 16, 2929. https://doi.org/10.1038/s41467-025-58234-2, 2025.

Jiang, Y., Chen, F., Gao, Y., He, C., Barlage, M., and Huang, W.: Assessment of uncertainty sources in snow cover simulation in the Tibetan plateau. *Journal of Geophysical Research: Atmospheres*, 125, e2020JD032674. https://doi.org/10.1029/2020JD032674, 2020.

Jiang, Y., Yang, K., Qi, Y., Zhou, X., He, J., Lu, H., Li, X., Chen, Y., Li, X.D., Zhou, B., Mamtimin, A., Shao, C., Ma, X., Tian, J., and Zhou, J.: TPHiPr: a long-term (1979–2020) high-accuracy precipitation dataset (1/30◦, daily) for the Third

https://doi.org/10.5194/egusphere-2025-6490
Preprint. Discussion started: 27 February 2026
© Author(s) 2026. CC BY 4.0 License.

Pole region based on high-resolution atmospheric modeling and dense observations. *Earth System Science Data*, 15, 621–638. https://doi.org/10.5194/essd-15-621-2023, 2023.

Lawrence, D. M., Fisher, R. A., Koven, C. D., Oleson, K. W., Swenson, S. C., Bonan, G., et al.: The Community Land Model version 5: Description of new features, benchmarking, and impact of forcing uncertainty. *Journal of Advances in Modeling Earth Systems*, 11, 4245–4287. https://doi.org/10.1029/2018MS001583, 2019.

Lawrence, P. J., and Chase, T. N.: Representing a new MODIS consistent land surface in the Community Land Model (CLM 3.0). *Journal of Geophysical Research*, 112, G01023. https://doi.org/10.1029/2006JG000168, 2007.

Leroux, N. R., Vionnet, V., and Thériault, J. M.: Performance of precipitation phase partitioning methods and their impact on snowpack evolution in a humid continental climate. *Hydrological Processes*, 37(11), e15028. https://doi.org/10.1002/hyp.15028, 2023.

Liston, G. E.: Representing subgrid snow cover heterogeneities in regional and global models. *Journal of Climate*, 17, 1381–1397. https://doi.org/10.1175/1520-0442(2004)017<1381:RSSCHI>2.0.CO;2, 2004

Liang, S., and Coauthors: The Global Land Surface Satellite (GLASS) Product Suite. *Bulletin of the American Meteorological Society*, 102, E323–E337, https://doi.org/10.1175/BAMS-D-18-0341.1, 2021.

Liu, L., and Ma, Y.: Improvement of Albedo and Snow-Cover Simulation during Snow Events over the Tibetan Plateau. *Monthly Weather Review*, 152, 705–724. https://doi.org/10.1175/MWR-D-23-0083.1, 2024.

Liu, R., Su, J., Zheng, D., Lü, H. and Zhu, Y.: Comprehensive assessment of various meteorological forcing datasets on the Tibetan Plateau: insights from independent observations and multivariate comparisons. *Journal of Hydrology*, 656, 133025. https://doi.org/10.1016/j.jhydrol.2025.133025, 2025.

Lopez-Moreno, J. I. and Stähli, M.: Statistical analysis of the snow cover variability in a subalpine watershed: Assessing the role of topography and forest, interactions. *Journal of Hydrology*, 348, 379–394. https://doi.org/10.1016/j.jhydrol.2007.10.018, 2008.

Lu, H., Zheng, D., Yang, K., and Yang, F.: Last-decade progress in understanding and modeling the land surface processes on the Tibetan Plateau. *Hydrology and Earth System Sciences*, 24, 5745–5758. https://doi.org/10.5194/hess-24-5745-2020, 2020.

Ma, X., and Wang, A.: Systematic Evaluation of a High-Resolution CLM5 Simulation over Continental China for 1979–2018. *Journal of Hydrometeorology*, 23, 1879–1897. https://doi.org/10.1175/JHM-D-22-0051.1, 2022.

Miao, X., Guo, W., Qiu, B., Lu, S., Zhang, Y., Xue, Y., and Sun, S.: Accounting for topographic effects on snow cover fraction and surface albedo simulations over the Tibetan Plateau in winter. *Journal of Advances in Modeling Earth Systems*, 14, e2022MS003035. https://doi.org/10.1029/2022MS003035, 2022.

Niu, G.-Y., and Yang, Z.-L.: An observation-based formulation of snow cover fraction and its evaluation over large North American river basins. *Journal of Geophysical Research*, 112, D21101. https://doi.org/10.1029/2007JD008674, 2007.

https://doi.org/10.5194/egusphere-2025-6490
Preprint. Discussion started: 27 February 2026
© Author(s) 2026. CC BY 4.0 License.

Orsolini, Y., Wegmann, M., Dutra, E., Liu, B., Balsamo, G., Yang, K., de Rosnay, P., Zhu, C., Wang, W., Senan, R., and Arduini, G.: Evaluation of snow depth and snow cover over the Tibetan Plateau in global reanalyses using in situ and satellite remote sensing observations. *The Cryosphere*, 13, 2221–2239. https://doi.org/10.5194/tc-13-2221-2019, 2019.

Prentice, I. C., Liang, X., Medlyn, B. E., and Wang, Y.-P.: Reliable, robust and realistic: the three R's of next-generation land-surface modelling. *Atmospheric Chemistry and Physics*, 15, 5987–6005. https://doi.org/10.5194/acp-15-5987-2015, 2015.

Qi, Q., Yang, K., Li, H., Ai, L., Wang, C., Wu, T.: Negative impacts of the withered grass stems on winter snow cover over the Tibetan Plateau. *Agricultural and Forest Meteorology*, 352, 110053. https://doi.org/10.1016/j.agrformet.2024.110053, 2024.

Swenson, S. C., and Lawrence, D. M. A new fractional snow-covered area parameterization for the Community Land Model and its effect on the surface energy balance. *Journal of Geophysical Research*, 117, D21107. https://doi.org/10.1029/2012JD018178, 2012.

Tang, Z. G., Wang, J., Li, H.Y., Yan, L. L.: Spatiotemporal changes of snow cover over the Tibetan plateau based on cloud-removed moderate resolution imaging spectroradiometer fractional snow cover product from 2001 to 2011. *Journal of Applied Remote Sensing*, 7, 073582. https://doi.org/10.1117/1.JRS.7.073582, 2013.

Toure, A.M., Rodell, M., Yang, Z., Beaudoing, H., Kim, E., Zhang, Y., and Kwon, Y.: Evaluation of the Snow Simulations from the Community Land Model, Version 4 (CLM4). *Journal of Hydrometeorology*, 17, 153–170. https://doi.org/10.1175/JHM-D-14-0165.1, 2016.

van Kampenhout, L., Lenaerts, J., Lipscomb, W. H., Sacks, W. J., Lawrence, D. M., Slater, A. G., and van den Broeke, M. R.: Improving the representation of polar snow and firn in the Community Earth System Model. *Journal of Advances in Modeling Earth Systems*, 9(7), 2583–2600. https://doi.org/10.1002/2017MS000988, 2017.

Verdin, K. L., and Greenlee, S. K. (1996). Development of continental scale digital elevation models and extraction of hydrographic features, paper presented at the Third International Workshop on Integrating GIS and Environmental Modeling. Santa Fe, New Mexico, 21–26 January, National Center for Geographic Information and Analysis, Santa Barbara, California.

Vionnet, V., Brun, E., Morin, S., Boone, A., Faroux, S., Le Moigne, P., Martin, E., and Willemet, J.-M.: The detailed snowpack scheme Crocus and its implementation in SURFEX v7.2. *Geoscientific Model Development*, 5, 773–791. https://doi.org/10.5194/gmd-5-773-2012, 2012.

Wang, A., Zeng, X., and Guo, D.: Estimates of Global Surface Hydrology and Heat Fluxes from the Community Land Model (CLM4.5) with Four Atmospheric Forcing Datasets. *Journal of Hydrometeorology*, 17, 2493–2510. https://doi.org/10.1175/JHM-D-16-0041.1, 2016.

Wang, C., Yang, K., Li, Y., Wu, D., and Bo, Y.: Impacts of Spatiotemporal Anomalies of Tibetan Plateau Snow Cover on Summer Precipitation in Eastern China. *Journal of Climate*, 30, 885-903. https://doi.org/10.1175/JCLI-D-16-0041.1, 2017.

https://doi.org/10.5194/egusphere-2025-6490
Preprint. Discussion started: 27 February 2026
© Author(s) 2026. CC BY 4.0 License.

Wang, W., and Coauthors: Characterizing Surface Albedo of Shallow Fresh Snow and Its Importance for Snow Ablation on the Interior of the Tibetan Plateau. *Journal of Hydrometeorology*, 21, 815–827. https://doi.org/10.1175/JHM-D-19-0193.1, 2020.

Xie, Z., Hu, Z., Ma, Y., Sun, G., Gu, L., Liu, S., et al.: Modeling blowing snow over the Tibetan Plateau with the Community Land Model: Method and preliminary evaluation. *Journal of Geophysical Research: Atmospheres*, 124, 9332–9355. https://doi.org/10.1029/2019JD030684, 2019.

Xie, Z., Hu, Z., Gu, L., Sun, G., Du, Y., and Yan, X.: Meteorological Forcing Datasets for Blowing Snow Modeling on the Tibetan Plateau: Evaluation and Intercomparison. *Journal of Hydrometeorology*, 18, 2761–2780. https://doi.org/10.1175/JHM-D-17-0075.1, 2017.

Yan, D., Ma, N., and Zhang, Y.: Development of a fine-resolution snow depth product based on the snow cover probability in the Tibetan Plateau: Validations and spatial-temporal analyses. *Journal of Hydrology*, 604,127027. https://doi.org/10.1016/j.jhydrol.2021.127027, 2022.

Yang, M., Wang, X., Pang, G., Wan, G., Liu, Z.: The Tibetan Plateau cryosphere: Observations and model simulations for current status and recent changes. *Earth-Science Reviews*, 190, 353-369. https://doi.org/10.1016/j.earscirev.2018.12.018, 2019.

Yang, K., He, J., Tang, W.J., Qin, J., and Cheng, C.: On downward shortwave and longwave radiations over high altitude regions: Observation and modeling in the Tibetan Plateau. *Agricultural and Forest Meteorology*, 150, 38-46. https://doi.org/10.1016/j.agrformet.2009.08.004, 2010.

Yang, K., Qi, Q., and Wang, C.: Possible impacts of vegetation cover increment on the relationship between winter snow cover anomalies over the Third Pole and summer precipitation in East Asia. *npj Climate and Atmospheric Science*, 6, 140. https://doi.org/10.1038/s41612-023-00467-3, 2023.

Yang, K.: Codes for manuscript "Optimization of snow cover fraction parameterization in the Community Land Model: implementation and preliminary validation over Tibetan Plateau", Zenodo [code], https://doi.org/10.5281/zenodo.18133296, 2026.

Zeng, J., Yuan, X., Ji, P., and Shi, C.: Effects of meteorological forcings and land surface model on soil moisture simulation over China. *Journal of Hydrology*, 603, 126978. https://doi.org/10.1016/j.jhydrol.2021.126978, 2021.

Zhang, P., Zheng, D., van der Velde, R., Wen, J., Su, Z.: Impact of model physics, meteorological forcing, and soil property data on simulating soil moisture and temperature profiles on the Tibetan Plateau. *Journal of Hydrology*, 654, 132809. https://doi.org/10.1016/j.jhydrol.2025.132809, 2025.

Zhang, X., Huang, A., Dai, Y., Li, W., Gu, C., Yuan, H., et al.: Influences of 3D sub-grid terrain radiative effect on the performance of CoLM over Heihe River Basin, Tibetan Plateau. *Journal of Advances in Modeling Earth Systems*, 14, e2021MS002654. https://doi.org/10.1029/2021MS002654, 2022.

https://doi.org/10.5194/egusphere-2025-6490
Preprint. Discussion started: 27 February 2026
© Author(s) 2026. CC BY 4.0 License.

Zhou, X., Ding, B., Yang, K., Pan, J., Ma, X., Zhao, L., et al.: Reducing the cold bias of the WRF model over the Tibetan Plateau by implementing a snow coverage-topography relationship and a fresh snow albedo scheme. *Journal of Advances in Modeling Earth Systems*, 15, e2023MS003626. https://doi.org/10.1029/2023ms003626, 2023.